Analysis of Experimental Results

Chapter V

Analysis of Experimental Results

5.1 Introduction :

The results which were obtained from various experimental measurements and which were presented in chapter IV are analysed in this chapter. The structural, optical and electrical characterisation data for crystalline material are presented in section 5.2. The optical characterisation results for hydrogenated amorphous silicon (a-Si:H) with various flow rates and various annealing temperatures are analysed and presented in section 5.3. In this section the effect of deposition rate and annealing temperature on the various parameters which were derived from the optical transmission spectrum has been studied and analysed. In section 5.4, the structural characterisation result from X-ray diffractogram and chemical bonding results from Fourier Transform Infra-Red Spectroscopy (FTIR) are studied and analysed. The effect of annealing temperature on coherence length and polycrystalline grain size (x-ray diffraction results) are analysed and presented in this section. The effect of annealing temperature on the integrated intensity, parameter R and oscillator strength (Γ) are studied and analysed in this section too. The above mentioned parameters are derived from Fourier Transform Infra-Red spectrum. In section 5.5, the electrical characterisation results for a-Si:H are studied and analysed. In this section the effect of annealing on activation energy, conductivity at room temperature and density of states at fermi level has been analysed. Finally the effect of hydrogen content on annealing temperature, optical gap, width of band tail (E_e) and refractive index in a-Si:H has been illustrated and analysed in section 5.6.

5.2 Analysis of Crystalline Semiconductor

5.2.1 Analysis of structural characterisation results.

Figure 4.1 (chapter IV) illustrates the x-ray difrractogram of crystalline silicon and a single sharp peak was observed at $2\theta \approx 69.20^0$, corresponding to diffraction from <400> plane having a spacing (d) ≈ 5.44Å. This was calculated by using Bragg's equation. The lattice spacing was obtained in this experiment by taking $2\theta \approx 69.20^0$ and the order of the spectrum m = 4.0. The lattice spacing for crystalline-Si as reported in the literature is 5.43Å for this plane [90]. The experimental result shows a very good agreement with the reported value showing that the crystal is a perfect one.

5.2.2. Analysis of optical characterisation results for crystalline semiconductors

Figure 4.2 (chapter IV) presents the data for the typical transmission spectrum of n-type crystalline-Si. From this spectrum, one can determine the absorption coefficient (α) by using the expression [8],

$$\alpha \approx \frac{4\pi k}{\lambda}$$

which was mentioned earlier in chapter II. k, the absorption constant which was calculated by using expression [8],

$$R = \frac{(1-n)^2 + k^2}{(1+n)^2 + k^2}$$

where n denotes the refractive index and R, the coefficient of reflection. Figure 5.1 presents the variation of the absorption coefficient (α) with the wavelength in (μm). The equations which were used to obtain these parameters have already been discussed in chapter III. From the graph (fig. 5.1) it was noticed that the absorption coefficient tends

to decrease with the wavelength and at around 1.12μm, the absorption coefficient will reach zero which corresponds to the energy gap of Silicon. The energy gap which was calculated from the experiment below, was found to be equal to 1.11eV and this value agrees well with reported one [90]. The equation which was used in the experiment to calculate E_g is as follows[91],

$$E_g = \frac{1.24}{\lambda(\mu m)} \qquad (5.2)$$

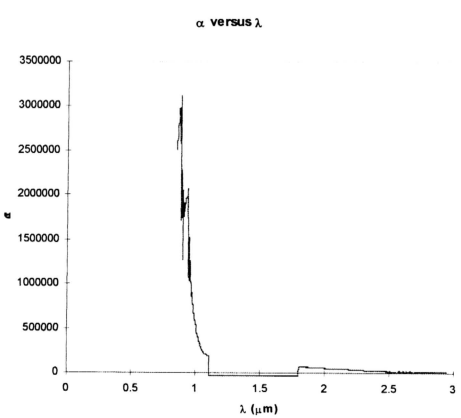

Figure 5.1 :Variation of absorption coefficient (α) with wavelength (λ in μm)

5.2.3. Analysis of electrical characterisation results for crystalline semiconductor

Figure 4.3 (chapter IV) presents the variation of $\log_{10}(\rho)$ against 1/T for an n-type Germanium sample. The measurement was carried out by using the four point probe

technique. The sample was placed on an aluminium substrate. The corrections to the measured resistivity were applied for the following causes:

i) finite sample width , and

ii) due to the probes being placed not very far away from the boundary

The equation for the calculation of the resistivity is given in chapter III. The energy gap (E_g) worked out to be 0.68 eV around room temperature. The standard value of energy gap (E_g) for Ge as reported is 0.66 eV at 300^0 K[91]. Figure 4.4 describes the variation of log(ρ) against 1/T for the sample of n-type Ge measured with the four point probe technique. But now the sample was placed upon a non-conducting (mica) base. The corrections due to the finite width and finite sample size were also applied in this case. The value of the energy gap has worked out to be 0.75 eV.

Figure (4.7-4.10), present the experimental data for the measurement of Hall coefficients for n and p-type of Ge sample. Fig. 4.7, presents the curve explaining the variation of the Hall Voltage as a function of the applied current for a steady magnetic field for n-type Ge. The variation is linear as expected. The fig. 4.8, on the other hand, presents the variation of the Hall voltage against the applied magnetic field for a steady current for the same sample. The curve is once again linear as expected. The Hall coefficient from the slope of latter curve is determined and is found to be 30.45×10^3 $cm^3 couloumb^{-1}$ as discussed in the chapter III. From the Hall coefficient data, the value of the carrier density, the electron mobility and the resistivity were estimated. They are respectively found to be $2.05 \times 10^{14} cm^{-3}$, $3045 cm^2 V^{-1} S^{-1}$, $10 \Omega cm$.. The standard value for the mobility of n-type Ge is 3900 $cm^2 V^{-1} S^{-1}$ [90].

Figure 4.9 presents the variation of the Hall voltage with the applied magnetic field for a steady current for p-type Ge sample. The curve is once again linear as expected. From the slope of this curve, the Hall coefficient was determined and found to be 18.28×10^3 $cm^3 couloumb^{-1}$. From this value, the hole density, the hole mobility and the resistivity of the sample were estimated. They are respectively found to be , 3.42×10^{14} cm^{-3}, 2031 $cm^2 V^{-1} S^{-1}$ and 9.0 Ωcm. The standard value for the hole mobility for p-type Ge is $1900 cm^2 V^{-1} S^{-1}$ [90].

Figure 4.6 presents the results for the variation of the log(ρ) as a function of 1/T for an n-type silicon sample. The method of measurement of resistivity in this case is a direct one. Two circular planar aluminium electrodes were deposited on both sides of a clean Si-wafer. The areas of the electrodes were measured by a micrometer scale. Some current is then passed through the sample by applying a voltage across the two electrodes. Both voltages and current were measured. Then from the width of the Si-sample , it is easy to estimate the resistivity. From the slope of the curve given in fig. 4.6 , the energy gap of the Si-sample was estimated. The energy gap found to be 0.41 eV. But the standard value for the energy gap of the Si at 300^0K is 1.12 eV[90]. The explanation for this discrepancy is presented below. During the deposition of electrodes on the Si-sample, a layer of Si dioxide could easily be formed on both sides of it. This SiO_2 layers would behave as ordinary resistors. It is well known that resistivity of a normal resistor increases with rising temperatures. We also know that, the resistance of semiconductors decreases with rising temperature. Hence, for a combination of an ordinary resistor and a semiconductor in series, we expect that the resistance of the combination should decrease at a lower rate with rising temperature than what is

expected of a normal semiconductor. That is the reason why the smaller slope of the curve in fig. 4.16, gives a low value for the energy gap.

Fig. (4.11-4.14) present the data for various parameters measured for n-type Si sample as a function of the frequency of the applied a.c. source. The parameters which were measured are, conductance , series and parallel capacitance and the loss coefficient of a Si sample. The sample was prepared in the same way as was employed for the d.c. case, mentioned earlier. It is interesting to note from the curve that the sample is exhibiting the a sort of resonance phenomenon. As the frequency increases from a low value, the conductance is found to be increasing, reaching a maximum at a particular frequency (resonance frequency). If the frequency is increased further , the conductance is observed to fall (fig. 4.14). Similar behaviour is also displayed by the series capacitance as a function of the frequency (fig. 4.11). The parallel capacitance on the other hand , starts dropping with a rise in the frequency reaching a zero value at the resonance frequency (fig. 4.12). Fig. 4.13 describes the variation of the loss coefficient as a function of the frequency. Since at series resonance, the resistance of the tank circuit approaches zero, the loss coefficient attains its maximum value at the resonance frequency. This resonance frequency was also found to be as a function of the annealing temperature. For the prepared sample the resonance frequency was found to be 1.3 MHz. On annealing the sample to 300 ^{0}C the resonance frequency rises to 3.2 MHz and when annealed at 500 ^{0}C, the resonance frequency drops to 1.7MHz.

5.3. Analysis on the growth rate of a-Si:H

Sample	Thickness ± 6 (nm)	Deposition Rate ±0.09 (nm/min)
5sccm on glass	725	8.06
25sccm on glass	1289	14.32
5sccm on crystalline-Si	422	4.69
25sccm on crystalline-Si	2470	27.44

Table 5.1 . Variation of thickness with deposition rate for 5 sccm and 25 sccm sample on glass and crystalline-Si substrate.

Table 5.1 presents the results of thickness measurements for a-Si:H on glass and crystalline-Si substrates for different flow and different deposition rates. The calculation of the thickness for a-Si:H on the glass substrate was obtained from the optical measurements whereas the thickness for a-Si:H on crystalline-Si substrate was obtained from the capacitance measurement. The techniques which were implemented to obtain these results have been presented in section 3.3.4. From the table 5.1, it is observed that the deposition rate of the film regardless of the substrate is significantly higher for the

higher silane flow rate. The net reaction for the plasma deposition of Si from SiH_4 is expressed by;

$$SiH_x \text{ (plasma)} \leftrightarrow Si \text{ (solid)} + xH \text{ (plasma)} \qquad [92]$$

From this expression, it is clear that deposition rate is higher when silane flow-rate is also higher. Increase of growth rate of a-Si:H film with flow-rate of silane in plasma glow discharge samples was also reported by Hirose et.al. [93]. The deposition rate however is higher on the glass substrate for the 5 sccm sample but is lower on the glass substrate for the 25 sccm sample. This is probably structure related. As discussed in section 3.3, the as prepared film for the 25 sccm sample is more crystalline than the 5 sccm sample. The <222> Bragg peak observed for the 25 sccm sample is sharper compared to the peak observed for the 5 sccm sample. It is obvious that the grain size for the 25 sccm sample is expected to be larger. The nanocrystallite structure was identified to be of SiO_2 with orthorhombic configuration. Being more crystalline, deposition of the 25 sccm sample is expected to be faster on the crystalline silicon substrate due to the more ordered structure. Thus being more amorphous, the 5 sccm sample is deposited faster on the glass substrates.

5.4 The effect of annealing temperature to the thickness of a-Si:H

Sample	Annealing Temperature (T_a, °C)	Thickness ± 5 (nm)
5 sccm on glass	as prepared	725
5 sccm on glass	300	518
5 sccm on glass	500	614
25 sccm on glass	as prepared	1289
25 sccm on glass	300	864
25 sccm on glass	500	919
5 sccm on crystalline-Si	as prepared	422
5 sccm on crystalline-Si	300	563
5 sccm on crystalline-Si	500	492
25 sccm on crystalline-Si	as prepared	2470
25 sccm on crystalline-Si	300	2180
25 sccm on crystalline-Si	500	4750

Table 5.2 : Variation of thickness with annealing temperature for 5 sccm and 25 sccm sample on glass and crystalline-Si substrate.

Table 5.2 presents the measured thickness for a-Si:H films on glass and crystalline-Si substrates in the as prepared and when annealed at 300°C and 500°C. From the table, it is observed that the thickness of the samples decrease when annealed at 300°C and increase once again when annealed at 500°C with the exception of the 5 sccm sample on crystalline-Si substrate. For this sample it is observed that the thickness

increases with the annealing temperature. Annealing is a form of heat treatment which was applied to the sample. When a heat treatment is applied on to the sample, the sample tends to rearrange and reconstruct the atomic structure of the crystal. Referring to figure 4.19, for 25 sccm sample on the glass substrate, the thickness of the film is found to be related to the volume fraction of crystallinity in the material which corresponds to the intensity of the Bragg peak present. The thickness increases with the volume fraction of crystal in the material. This is true when the preferential orientation of the plane is the <222>. When the preferential orientation of the plane is the <200>, as for the 5 sccm sample, the thickness is found to decrease when the volume fraction of crystallinity in the material increases (figure 4.18). However, being totally amorphous when annealed at 500^0C, the increase in the thickness is not so significant. The thickness dependence on the volume of fraction of crystallinity in the material for the a-Si:H film deposited on the crystalline silicon cannot be confirmed since the x-ray diffractogram in this case was not available.

5.5 Analysis of the refractive index values

Sample	Annealing Temperature (T_a °C)	Refractive Index (n) ±0.05	H%±0.1 Optical
5 sccm	as prepared	2.34	34.8
5 sccm	300	2.39	20.3
5 sccm	500	2.87	14.6
25 sccm	as prepared	2.42	32.2
25 sccm	300	2.73	26.2
25 sccm	500	3.05	20.4

Table 5.3 : Variation of refractive indices with annealing temperature for the 5 sccm and 25 sccm sample on glass substrate.

Table 5.3 presents the calculated refractive indices of a-Si:H thin films deposited on the glass substrates for the 5 sccm and 25 sccm conditions in case of as prepared and when annealed at 300^0C and 500^0C. The H% calculated from the optical spectrum are also tabulated. From table 5.3, it is observed that the refractive indices of the sample for both the flow rates increase with the annealing temperatures. Generally the refractive index of the sample depends upon the deposition rate. It was observed that the refractive index of the 25 sccm sample is higher than the 5 sccm sample. This suggests that the higher deposition rate of 25 sccm sample could have resulted in a more compact crystal structure for the film. Compact structures can result in denser films thus giving rise to higher refractive indices. Refractive indices are higher for denser materials [94] (eg. Refractive indices of most metals are higher than those of non-metals because metals are materials with higher densities). When annealed, hydrogen is evolved from the film, leaving behind more of unbonded Si atoms. This naturally increases the density of the film. This also explains the increasing trend of the refractive index of both the films when annealed as observed in table 5.3. The refractive index is also observed to be dependent on the H% as calculated from the optical spectrum. Increase in the refractive index is observed when the H% decreases. Thus it can be deduced that decrease in this H% results in the increase in the density of the film. However, other factor also has influence on the film density. This is clearly observed from the higher refractive index of the annealed 25 sccm film even though the H% (optical spectrum) is higher. Presence of voids in film also reduce the film density.

5.6 The effect of annealing temperature on polycrystalline grain size (D) (x-ray diffraction results)

Samples	Annealing Temperature $T_a{}^0C$	Polycrystalline Grain Size D ± 0.02 (nm)
5 sccm	as prepared	15.28
5 sccm	300	17.43
5 sccm	500	not detected
25 sccm	as prepared	57.27
25 sccm	300	19.87
25 sccm	500	34.39

Table 5.4 : Variation of polycrystalline grain size(D) for the 5 sccm and 25 sccm sample with various annealing temperatures.

Table 5.4 depicts the polycrystalline grain size(D) for 5 sccm and 25 sccm, as prepared sample and when annealed at 300^0C and 500^0C. The grain size (D) could be calculated by using the following equation [87],

$$L = \frac{0.9\lambda}{(\Delta 2\theta)\cos(\theta_0)} \qquad (5.3)$$

where L is the crystallite size or coherence length , λ is the wavelength of x-ray diffraction , θ_0 is the angle of reflectance of the peak and ($\Delta 2\theta$) is the full width at half-maximum (FWHM). The grain size, D then can be computed as :

$$D = \frac{4L}{3} \qquad (5.4)$$

From the table 5.4, it was observed that the nanocrystal grain size for the 25 sccm as prepared sample is comparatively larger than the grain size of the 5 sccm sample. These nanocrystals which were formed in both the cases correspond to SiO_2 which was identified from the Bragg peak in chapter IV (fig. 4.17). The Bragg peak which was

observed in 25 sccm sample is well-defined and sharp compared to that found in 5 sccm sample. This indicates that for the high silane flow-rate, the sample has more oxygen trapped which leads to higher volume fraction of crystalline material.

When the 5 sccm sample was annealed at 300°C, the SiO_2 grain size increases and this shows that the volume fraction of crystalline material in 5 sccm sample increases when annealed at this temperature. This is confirmed by Bragg peak in fig. 4.18, where the intensity of the peaks corresponding to <200> plane was found to increase when annealed at this temperature. This observation indicates that the network construction and the recrystallization process occurs in the sample at this annealing temperature and this leads to the formation of a larger grain size of the SiO_2 nanocrystal. When the sample is annealed at 500°C, the nanocrystal which was observed in the as prepared condition and when annealed at 300°C is no longer observed. This is also confirmed by the Bragg peak in fig. 4.18 corresponding to <200> plane. This is found to collapse when annealed at this temperature. The film then totally becomes amorphous in nature. This indicates that the SiO_2 bonds may have transformed to other bonding scheme such as Si-O-Si-H bonding modes when annealed at 500°C.

For the 25 sccm sample, the nanocrystal grains which correspond to SiO_2, decreased in size when annealed at 300°C. This observation was further confirmed by the decrease in intensity of the Bragg peak (fig. 4.19) corresponding to the planes <200> and <222> and disappearance of Bragg peak for the planes <261> and <222>. These indicate that the SiO_2 bonds in this sample may have transformed to Si-O-Si-H type. When the sample was annealed at 500°C, the grain size of the nanocrystal increases but becomes smaller than in the as prepared case. This was also confirmed by the sharp Bragg peaks

corresponding to planes <261> and <222> which reappear (fig. 4.19). This observation indicates that recrystallization process has occurred in the sample which leads to a larger grain size of SiO_2 nanocrystal in the material.

5.7 Analysis of the Fourier Transform Infra-Red (FTIR) Spectroscopy results

Sample	T_a °C	I_{640} ±0.07	I_{656} ±0.07	I_{880} ±0.07	I_{900} ±0.07	I_{1070} ±0.07	I_{2000} ±0.07	I_{2100} ±0.07	I_{2260} ±0.07	R % ±0.07
5 sccm	as prep.	1050.57	nd	65.30	241.26	17.92	265.02	189.75	33.45	33.62
5 sccm	300	1213.40	nd	64.04	nd	95.69	113.57	99.86	23.18	38.83
5 sccm	500	660.91	nd	42.36	nd	77.84	nd	nd	19.16	21.15
25 sccm	as prep.	446.40	22.02	37.88	nd	29.98	117.7	1403.2	nd	14.28
25 sccm	300	504.80	nd	19.50	nd	239.50	113.90	122.46	3.06	16.15
25 sccm	500	18.32	nd	2.55	nd	8.51	nd	nd	1.90	0.58

nd - not detected

Table 5.5 : Variation of integrated intensities under the peaks and the hydrogen content with annealing temperature for 5 sccm and 25 sccm sample.

Table 5.5, presents the integrated intensities under the absorption peaks of the FTIR spectra and the hydrogen contents for 5 sccm and 25 sccm, as prepared samples and when annealed at 300°C and 500°C. From the table 5.5, the integrated intensity at 640 cm^{-1} which corresponds to Si-H wagging for both the samples was observed to increase when annealed at 300°C and decrease when it was further annealed at 500°C. The integrated intensity of this absorption peak is directly proportional to the hydrogen content in the film. The hydrogen content is calculated using the equations (3.64) and (3.65). The increase in the hydrogen content for both samples when annealed at 300°C may be due to the presence of IR inactive hydrogen in the as prepared sample which

becomes IR active when annealed at 300^{0}C. When the samples were annealed at 500^{0}C, the hydrogen content decreases because of the evolution of hydrogen from the Si-H_2 bonds near the surface, leaving behind hydrogen bonded in the Si-H and Si-H_2 bonding configurations in the bulk of the film [78,85]. The I_{2000} and I_{2100} correspond to the integrated intensities of the Si-H stretching and Si-H_2 / $(Si-H_2)_n$ stretching bands respectively. When annealed at 300^{0}C the I_{2000} and I_{2100} for both samples decreased. The I_{2000} and I_{2100} which were observed in the as prepared sample is no longer observed when both the samples were annealed at 500^{0}C. The decrease and complete the disappearance of I_{2000} and I_{2100} for both the samples are related to hydrogen being evolved from the bonding sites. The decrease of I_{2000} and I_{2100} at Ta $\approx$ 300^{0}C is related to the clustered Si-H and/or bulk $(Si-H)_n$ groups. The pronounced decrease above 300^{0}C is due to Si-H sites on or near the surface [78,85]. The final disappearance of I_{2000} and I_{2100} at 500^{0}C for both samples is related to the evolution of hydrogen from the bulk Si-H sites or the transformation of such groups into the Si-H back bonded to O sites at ~ 2364 cm^{-1} [78,84,85].

The integrated intensity at 890 cm^{-1} (I_{890}) corresponds to $(Si-H_2)_n$ bending scissors. For both sample I_{890} decreases when the sample was annealed at 300^{0}C and 500^{0}C. The initial decrease of I_{890} at 300^{0}C is related to the disruption of $(Si-H_2)_n$ and isolated Si-H_2 bonds. The final decrease in I_{890} for both sample is related to the diffusion delayed evolution of hydrogen from the bulk Si-H_2 sites [78]. It should be mentioned here that the evolution of hydrogen occurs at $T_a \approx$ 300^{0}C from $(Si-H_2)_n$ and at $T_a \approx$500^{0}C from the bulk Si-H and Si-H_2 sites respectively. From the hydrogen content, it can be inferred that $(Si-H_2)_n$ bonds which breaks at ~ 300^{0}C make almost no contribution to the

hydrogen content derived from I_{640} since at this point the hydrogen concentration increases when annealed.

The integrated intensity at 1100 cm^{-1}(I_{1100}) corresponds to Si-O stretch and this oxygen is due to the contamination of the film. For 5 sccm sample I_{1100} is observed to increase when annealed at 300^0C and decreased when annealed at 500^0C. The presence of SiO_2 in the as prepared sample is confirmed by the x-ray diffraction peaks which were identified to be due to SiO_2 nanocrystal, as observed in fig. 4.18. When the sample is annealed at 300^0C, the amount of SiO_2 in the a-Si matrix increases and this is further confirmed by the formation of a larger size crystal of SiO_2 in a-Si structure. The peak intensity was observed to increase when annealed at 300^0C in fig. 4.18. When the samples were annealed at 500^0C, the amount of contaminated oxygen in the a-Si matrix decreases and this is consistent with the disappearance of x-ray diffraction peaks as observed in figure 4.19. For 25 sccm sample I_{1100} at annealing temperature 500^0C is very much smaller then the as prepared sample. It can be concluded that the amount of oxygen in 500^0C annealed sample is smaller as compared to the as prepared sample. This is again consistent with the reduction in the intensity of the sharp x-ray diffraction peaks in figure 4.19 as compared to the as prepared sample.

5.8 The effect of annealing temperature on the R parameter

Sample	Annealing Temperature (T_a °C)	R ±0.09
5 sccm	as prepared	0.42
5 sccm	300	0.47
5 sccm	500	nd
25 sccm	as prepared	0.54
25 sccm	300	0.53
25 sccm	500	nd

nd - not detected

Table 5.6 : Variation of parameter R with annealing temperature for 5 sccm and 25 sccm sample.

Table 5.6, presents the parameter R for 5 sccm and 25 sccm as prepared sample and when annealed at 300^{0}C and 500^{0}C. Parameter R is defined by the following equation [85];

$$\mathbf{R} = \frac{I_{2100}}{I_{2000} + I_{2100}} \qquad (5.5)$$

where $I_{2000}$is the integrated intensity at 2100 cm^{-1} and I_{2000} is the integrated intensity at 2000 cm^{-1}. The parameter R is proportional to the fraction of hydrogen bonded in some sort of microstructures (multivacancies, small voids, etc.) leading to a large density deficiency [85]. For the 5 sccm sample, the parameter R increases when annealed at 300^{0}C, suggesting increase in hydrogen bonded in some sort of microstructure. This is consistent with the x-ray diffraction spectrum of figure 4.18 where the intensity of the Bragg peak increases when annealed at this temperature. When annealed at 500^{0}C, the film becomes totally amorphous, as observed from the x-ray diffraction results (figure 4.18) and the disappearance of absorption peaks at 2100 cm^{-1} and 2000 cm^{-1} at this

annealing temperature confirms that the parameter R is also related to the presence of microstructures in the film. The 25 sccm as prepared sample has a higher R value as compared to the 5 sccm sample. An interesting relationship is observed between the R values and the intensity of the Bragg peak for the <200> plane (refer figure 4.17). The intensity of the Bragg peak for the 25 sccm as prepared sample is clearly higher than that for the 5 sccm as prepared sample and thus the R values are correspondingly higher for the former as compared to the latter. When annealed at 300^0C, the intensity of this peak decreases and so does the R value. In agreement with the observed trend for the R value and the intensity of the Bragg peak variation corresponding to the <200> plane, the R value becomes zero when annealed at 500^0C and the Bragg peak for this plane is also found to disappears when annealed at this temperature (refer figure 4.19). The intensity of the Bragg peak corresponding to the <222> plane has no effect on the R value. This suggests that the hydrogen bonded to the microstructure in the film are bonded to the <200> plane.

5.9 Effect of annealing temperature on the density of states [$N(E_f)$] at the fermi level

The density of states at fermi level, $N(E_f)$ is determined from the a.c. conductivity results using equation 3.49. The conductivity at a fixed frequency of 10^6 Hz is plotted against the measurement temperature. The N(Ef) is then obtained from the slope of this plot where the slope corresponds to:

$$\text{slope} = \left(\frac{\pi}{3}\right) e^2 k \left(N(E_f)\right)^2 \alpha^{-5} \omega \left[\ln\left(\frac{\upsilon_{ph}}{\omega}\right)\right]^4 \qquad (5.6)$$

The values of the parameters are given in section 3.3.4 (B).

Sample	T_a ^{0}C	N(Ef) ± 0.06 x10^{19} $ev^{-1}cm^{-3}$
5 sccm	as prepared	$1.38x10^{19}$
5 sccm	300	$2.35x10^{19}$
5 sccm	500	$4.57x10^{19}$
25 sccm	as prepared	$1.28x10^{19}$
25 sccm	300	$1.57x10^{19}$
25 sccm	500	$1.82x10^{19}$

Table 5.7 : Variation in the density of states [$N(E_f)$] with annealing temperature for 5 sccm and 25 sccm sample

Table 5.7 presents the density of states at fermi level [$N(E_f)$] for both the 5 sccm and 25 sccm as prepared samples and when annealed at 300^0C and 500^0C. From the table, it is observed that the density of states at fermi level for both samples increase with the annealing temperature. This increase is related to the amount of hydrogen atoms incorporated in the a-Si matrix. When the samples are annealed at higher temperatures, hydrogen evolution occur and the evidence for this evolution has already been mentioned in the previous sections. The evolution of hydrogen creates dangling bonds and this dangling bonds concentration will increase with the annealing temperatures. The formed dangling bond will transform into shallow matrix defects near the fermi level. These defect states near the fermi level increases the density of states $N(E_f)$ [95-97]. This is consistent with the results tabulated in table 5.7. As the annealing temperature increases, $N(E_f)$ increases.

5.10 Analysis of activation energy results and the d.c. conductivity

Sample	T_a ^{0}C	$E_c - E_f \pm 0.06$ (eV)	$\sigma_{RT} \pm 0.04$ x10^{-6} SΩ^{-1}
5 sccm	as prepared	0.56	1.16×10^{-6}
5 sccm	300	0.44	1.43×10^{-6}
5 sccm	500	0.26	6.34×10^{-6}
25 sccm	as prepared	1.03	3.47×10^{-7}
25 sccm	300	0.54	1.30×10^{-6}
25 sccm	500	0.30	3.59×10^{-6}

Table 5.8 : Variation of activation energy and conductivity at room temperature with annealing temperature for 5 sccm and 25 sccm sample.

Table 5.8 tabulates the activation energy and the conductivity at room temperature for 5 sccm and 25 sccm as prepared samples and when annealed at 300^{0}C and 500^{0}C. The calculation techniques which were used to obtain the activation energy and the conductivity of the as prepared and annealed samples at 300^{0}C and 500^{0}C have been presented in section 3.3.4 (A). For both the samples, the activation energy ($E_c - E_f$) decreases when the samples were annealed at 300^{0}C and 500^{0}C. The decrease is caused by an increase in the density of states [$N(E_f)$]. The increase in the density of states will result in more electrons being trapped in the states at the fermi level. This results in the shift in the fermi level towards the conduction band. The conductivity increases correspondingly with the decrease in the activation energy. This is consistent since at lower activation energies one should expect to observe higher conductivity in the sample. The conductivity of the 25 sccm as prepared sample is lower than that of 5 sccm as prepared sample. This supports the fact that the activation energy is also significantly larger for the 25 sccm as prepared sample and also the $N(E_f)$ is correspondingly lower for the 25 sccm as prepared sample which clearly supports the above argument.

5.11 Analysis of hydrogen content in the a-Si:H

Sample	T_s °C	H%±0.1 Optical	H%±0.07 FTIR
5 sccm	as prepared	34.8	33.62
5 sccm	300	20.3	38.83
5 sccm	500	14.6	21.15
25 sccm	as prepared	32.2	14.28
25 sccm	300	26.2	16.15
25 sccm	500	20.4	0.58

Table 5.9 : Variation of hydrogen content (calculated from optical measurement and FTIR measurement) with annealing temperature for 5 sccm and 25 sccm sample.

Table 5.9 presents the hydrogen concentration (H%) which was obtained from optical transmission spectrum and the FTIR spectrum for 5 sccm and 25 sccm samples at different annealing temperatures. From table 5.9, it is observed that the hydrogen content obtained from the optical and the FTIR spectra are different. This is due to the fact that the hydrogen content derived from optical data accounts for hydrogens at all bonding sites including to those bonded to Si-O bonds. The hydrogen content obtained from the FTIR spectrum consists only of hydrogen at the Si-H bonding sites only. Langford et.al [98] claims that this hydrogen content includes microvoid concentration in the film. This hydrogen content is overestimated up to a certain magnitude dependent of microvoid content in the film.

For the 5 sccm as prepared sample, there is no significant difference between the hydrogen content derived from optical and the FTIR calculations. This is due to the presence of low fraction of SiO_2 bonds in the sample and this is indicated by the low integrated intensity at wavenumber 1100 cm^{-1} which corresponds to this bonding sites (as observed in table 5.5). Due to the low SiO_2 bonds, there is a low possibility for the hydrogen in the sample to be attached with these SiO_2 bonds. When the 5 sccm sample

was annealed at 300^{0}C and 500^{0}C, the hydrogen content derived from the optical calculations is lower compared to that obtained from the FTIR spectrum. This strongly indicates that the presence of microvoids is more significant in the 5 sccm film even when annealed.

For 25 sccm (as prepared and annealed at 300^{0}C and 500^{0}C) samples, the hydrogen content obtained from the optical spectrum is much higher than the hydrogen content obtained from the FTIR spectrum. This is due to the fact that the presence of oxygen contamination in the 25 sccm sample as-prepared and even when annealed (refer table 5.5) is more significant in the 25 sccm sample. So, the possibility of more hydrogen being attached to this bond is higher.

For both the 5 sccm and 25 sccm samples, the hydrogen content derived from the FTIR method increased when annealed at 300^{0}C. This indicates that the presence of IR inactive hydrogen in the film is higher. When both samples were annealed at 500^{0}C, the hydrogen content decreases indicating that the evolution of hydrogen atoms is taking place from near surface bonding SiH and/or SiH_2 bonding sites leaving behind hydrogen bonded in the SiH and SiH_2 bonding configurations in the bulk.

For both the 5 sccm and 25 sccm samples, the hydrogen content derived from optical data decrease when annealed at 300^{0}C and 500^{0}C, indicating that the evolution of hydrogen is taking place at various bonding sites including those bonded to Si-O bonds.

5.12 Optical Gap of a-Si:H (analysis)

Sample	T_a °C	H%±0.1 Optical	H%±0.07 FTIR	E_g±0.01 (eV)
5 sccm	as prepared	34.82	33.62	2.04
5 sccm	300	20.34	38.83	1.98
5 sccm	500	14.64	21.15	1.67
25 sccm	as prepared	32.22	14.28	2.14
25 sccm	300	26.21	16.15	2.12
25 sccm	500	20.39	0.58	1.64

Table 5.10 : Variation of optical energy gap(E_g) with H% in the sample for 5 sccm and 25 sccm sample as-prepared and annealed at 300°C and 500°C

Table 5.10 tabulates the optical energy gap (E_g) and the hydrogen content obtained from the optical and the FTIR transmission spectrum for 5 sccm and 25 sccm samples. The decrease in E_g when annealed at 300°C is not significant for both samples. Both samples show a significant decrease in E_g when annealed at 500°C. The change in the hydrogen content calculated from the FTIR spectrum is also insignificant when annealed at 300°C and this hydrogen content also shows a significant decrease when annealed at 500°C for both samples. The hydrogen content calculated from optical spectrum demonstrate significant decrease when annealed at 300°C and 500°C for both samples. Thus, the E_g shows a strong dependence on the hydrogen content calculated from the FTIR spectrum in both samples. The small decrease in E_g observed when annealed at 300°C is due to the fact that the healing of pure matrix defects is over-shadowed by the transformation of hydrogen related defects into the pure matrix defects. When annealed at 300°C, the slight decrease in E_g is observed due to the removal of hydrogen from $(SiH_2)_n$ bonding sites at the surface. The process of hydrogen evolution at this annealing temperature results in the creation of dangling bonds which create defect

states near the fermi level which has insignificant effect on the energy gap. These hydrogen atoms are removed from the $(SiH_2)_n$ bonding sites as observed from the decrease in the integrated intensity at 890 cm^{-1} when annealed at this temperature (table 5.5). Thus, hydrogen removed from $(SiH_2)_n$ sites creates dangling bond which results in the increase in $N(E_f)$, ie. states at the fermi level which is confirmed from results in section 5.9. When both samples were annealed at 500^0C, a significant decrease in the optical energy gap was observed. This significant decrease at 500^0C is due to hydrogen evolved from Si-H bonding sites which is confirmed from the significant decrease in hydrogen content using the FTIR spectrum. This removal of hydrogen from these sites create pure matrix defects in the mobility gap which leads to the significant decrease in E_g [99, 100, 101].

5.13 Analysis Urbach Tail Band Width of a-Si:H

Sample	T_a °C	D (nm)	E_e ±0.02 (eV)
5 sccm	as prepared	15.28	0.11
5 sccm	300	17.43	0.14
5 sccm	500	not detected	0.24
25 sccm	as prepared	57.27	0.10
25 sccm	300	19.87	0.07
25 sccm	500	34.39	0.08

Table 5.11 : Variation of width of the band tail (E_e) with hydrogen content in the sample for 5 sccm and 25 sccm sample at different annealing temperature

The Urbach tail band width, E_e quantifies the magnitude of disorder in the film [102]. Higher E_e values indicates the film structure is more disordered. Table 5.11 presents the values of E_e and the grain size, D of the microcrystallite grain structure in the film. The calculation for this value is described in section 3.3.3 (II). From table 5.11, it

appears there is some sort of relationship between grain size of the microcrystallite grain structure in film and the magnitude of disorder in the film. Larger grain sizes results in a more ordered film while amorphous film produce a more disordered structure. The higher flow-rate sample produces small E_e values even when annealed and the grain size values are consistently larger even when annealed. However, other factors also contribute to the disorder in the film since the magnitude of E_e is almost the same for both as-prepared film but the grain size of the 25 sccm film is more than triple the grain size of 5 sccm sample.